Electroosmotic Flow Control in Micro Channels Produced by Scanning Excimer Laser Ablation

Frank WAGNER and Patrik HOFFMANN

Institute of Applied Optics, BM, Swiss Federal Institute of Technology Lausanne,
CH – 1015 Lausanne EPFL, Switzerland
E-mail: Patrik.Hoffmann@epfl.ch

Excimer laser ablation of a scanned substrate can be used for prototyping of lab-on-a-chip microfluidic channels [1]. Here, the relationship between the wetting properties of the channels and the irradiation conditions is described. The wetting properties are quantified by electroosmotic flow measurements in channels, produced with different conditions of scanning ablation. The observed variations can be explained in terms of a competition between a direct and an indirect redeposition pathway for the debris.

Keywords: Micro machining, surface modification, microfluidics, electroosmotic flow.

1. Introduction

Excimer laser ablation of polymers is well known to produce high quality structures in nearly all polymers, as it was first described in 1982 [2]. As mentioned recently by Rossier *et al.* [3], a drastic increase in hydrophilicity of ablated micro channels in poly(ethylene terephthalate) (PET) can be achieved by scanning the substrate. This makes excimer laser ablation a versatile tool for rapid prototyping of micro fluidic systems, as for example lab-on-a-chip devices.

In such devices, a sample solution (usually aqueous) is injected, pumped, separated and eventually analyzed by electrochemical means. Channels for these applications need to meet special requirements in their surface properties in order to optimize the efficiency of the final device. We have already investigated in detail the influence of the irradiation conditions on the surface structure of the channel floor and of the ramps, forming at the beginning and at the end of the channels [4]. We also observed an enhanced redeposition of debris in the channel, depending on the conditions during the ablation [5].

In this paper, we show how the scanning ablation parameters influence the electroosmotic flow in PET micro channels. Further we propose an explanation for the observed effect.

2. Scanning ablation

In order to produce micro channels, which are longer than the beam width on the sample, one can imagine two modes of fabrication. (i) One can drill one rectangular hole using a common mask projection technique, stop the laser, move the substrate, drill the next hole in contact with the first one and so on. This mode of channel fabrication will be called "static ablation". (ii) Alternatively, the substrate can be moved with the appropriate speed v while it is irradiated by the laser, in order to produce channels of the required depth d_{tot}. Further on, we will refer to this method as "scanning ablation".

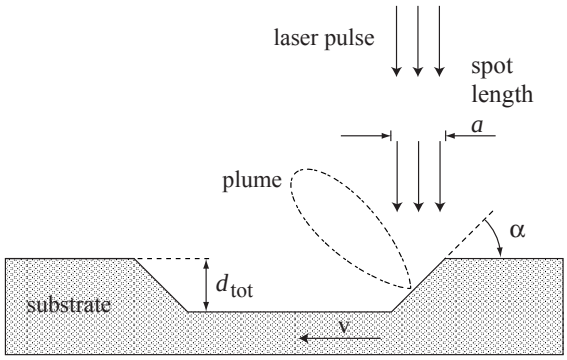

Fig. 1 Schematic diagram showing the parameters of scanning ablation

When using scanning ablation, ramps form at the beginning and at the end of the channels during the fabrication. Only the end ramp is irradiated. The angle α, that it forms with the original sample surface, is given by the depth of the channel d_{tot} and the length of the irradiated spot a in the scanning direction (Fig. 1), i.e. $\alpha = \arctan(d_{tot}/a)$. The depth of the channel can be expressed by $d_{tot} = n \times h(\Phi)$, where n is the number of pulses used in static ablation for one hole, and $h(\Phi)$ the ablated thickness per pulse at fluence Φ. Given the pulse repetition rate f, n and a, the appropriate scan speed v can be derived: $v = f \times a / n$.

3. Experimental

3.1 Substrates and laser

Two types of substrates were used: (i) Biaxially stretched poly(ethylene terephthalate) (PET) foil, in which one stretching direction dominated over the other (thickness 100 μm, Melinex S, ICI). (ii) Amorphous unstretched PET (thickness 500 μm, Mylar, Goodfellow).

These two substrates were irradiated with a standard ArF excimer laser (193 nm, 20 ns, LPX 205, Lambda-Physik) as already described [4].

3.2 Channel production

We used n = 200 pulses and a width of 40 μm for all channels. The channel length between the two reservoirs was 15 mm. The reservoirs were drilled by static laser ablation. In both substrates, we produced 38 μm deep channels by using different spot lengths a and scanning speeds v. This resulted in a change of the ramp angle α during the ablation (Table 1).

Table 1 Corresponding values for the spot length a (μm) and the ramp angle α (degrees).

a (μm)	1000	500	200	100	50
α (°)	2.0	4.3	11	22	42

For the stretched samples we used holes of 1000 μm times 40 μm that we drilled completely through the sample as reservoirs. After channel and reservoir fabrication by laser ablation, the samples were laminated with a poly(ethylene) (PE) on PET lamination at 130°C in order to close them.

In the unstretched substrates, the use of through-drilled holes led to insufficient quality of the electroosmotic measurement data, because the reservoir volume / channel volume ratio became too high. Therefore, for this kind of substrate, the channels were first drilled, then laminated and finally the lamination was opened by the laser. A drop of solution placed on the openings of the lamination then represents the reservoir. Measurements (< 3min.) were carried out directly after placing the drops, so that concentration changes due to solvent evaporation can be neglected.

In the stretched samples, the static structure, developed perpendicularly to the main stretching direction [6]. Its amplitude and period are about 3 μm. We produced two series of channels in the stretched substrate; in one series, we aligned the structure with the channel direction ("longitudinal" series) and, in the other series, the structure was perpendicular to the channel direction ("transversal" series). As recently described, the static structure transforms to the scanning structure for $\alpha \geq 11°$ [5]. This leads to a smoother channel surface in the micron range. As expected, the channels in the unstretched substrate did not show any structure in the micron range.

In all three series, the debris contribution became important for $\alpha \geq 22°$ and added nanometer scale roughness and porosity to the channels [5].

3.3 Electroosmotic flow measurement

The electroosmotic flow was measured using Huang's current monitoring method [7]. We placed drops (10 μl) of phosphate buffer (pH = 7.2, Sigma) in each reservoir. The total salt concentration of the buffer in the two reservoirs differed slightly (10 mMol/l, 8 mMol/l). While applying the electric field that induced the electroosmotic flow, the resistivity of the channel was monitored by measuring the electrical current. The resistivity of the channel at a given time depends on the percentage of the channel filled with the low resistivity (high concentration) buffer and the percentage of the channel filled with the high resistivity (low concentration) buffer. The measurement of the channel resistivity as a function of time thus indicates the motion of the interface formed by the two liquids.

For all measurements, we applied a driving electrical field of 20 kV/m and all cited literature values are converted to this value for better comparison. The measured electrical current was about 4 μA and hence heating effects can be neglected.

4. Results and discussion

4.1 General observations

The electroosmotic flow velocity in the channels varied as a function of the ramp angle by about 25% in all three series (Fig. 2). In almost all cases the maximum flow velocity was reached at $\alpha = 4.3°$ and was approximately as high as the value for fused silica capillaries (10×10^{-4} m/s [7]). All the data represented in Fig. 2 resulted from laminated channels. This PE-lamination is identical for all channels and thus smoothes the flow velocity data. This means that the observed variations are lower than the variations that would be observed if all four walls of the channels were ablated surfaces.

No significant differences could be found between the longitudinal and the transversal series. In other words, the orientation of the micrometric structure has no measurable influence on the electroosmotic flow in our experiments.

Comparing our values ($\alpha = 2°$) with the value published by Roberts *et al.* [8], we observe in absence of the micrometric structure a slightly faster electroosmotic flow. In more detail the values of the longitudinal and transversal series of 8.3×10^{-4} m/s and 8.5×10^{-4} m/s respectively are in excellent agreement with the value of Roberts *et al.* (8.4×10^{-4} m/s), whereas the value of the series without structure of 9.9×10^{-4} m/s is 18% higher. However, in order to confirm this value, further investigations are necessary.

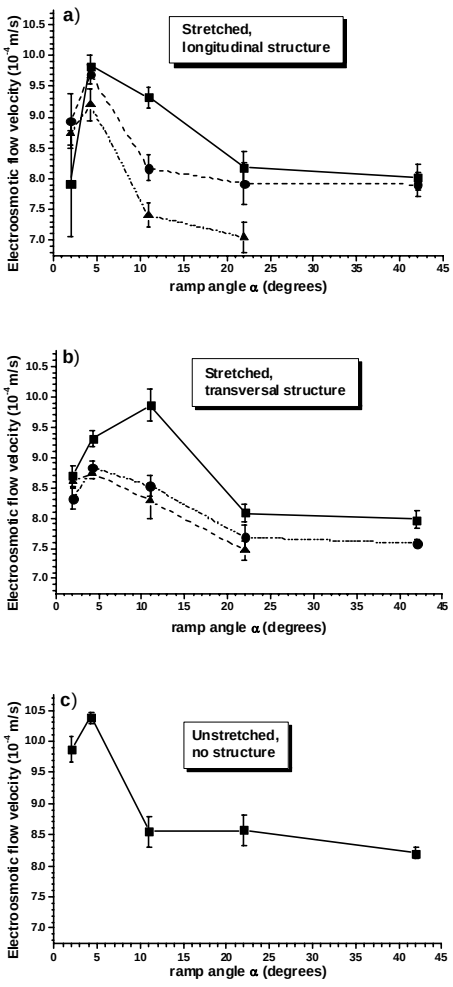

Fig. 2 Electroosmotic flow velocity (@ 20 kV/m) as a function of the ramp angle α. Figures **a** and **b** show the series produced in the stretched substrate. Figure **c** shows the series produced in the unstretched substrate. (For further details see experimental section.) Different curves in one graph correspond to channels produced or analyzed on different days. The standard errors for 3 pairs of drops and 4 measurements per drop pair in the same channel are indicated.

4.2 Explication of the maximum

The maximum flow velocity, observed in all substrates around $\alpha = 4.3°$, can be interpreted in terms of variations in the ζ-potential of the channels. As we always used the same buffer, variations in the ζ-potential are directly related to variations in the surface charges or polarity of the channel surfaces. These surface properties also determine the water wetting behavior of the polymer and of the ablated polymer.

Lazare *et al.* reported a decreasing O/C-ratio in XPS measurements after static ablation of PET at 193nm wavelength [9]. This is in good agreement with their observation that the water contact angle increases, from 68° on unirradiated PET to 105° on the ablated surface. This data indicates clearly that PET has a low ζ-potential compared to clean fused silica, that is wetted by water (contact angle = 0°, [10]), and that static ablation further decreases the ζ-potential.

However, the ζ-potential of channels produced by scanning ablation is determined by the debris. The debris can be more or less charged or composed by polar reaction products, which are formed during the collisions of the ejected ablation products with oxygen in air [11].

In the case of static ablation, collisions with the ambient gas are the main reasons for redeposition of the debris on the substrate [12]. The left part of Fig. 3 shows water condensed by breathing out near a statically ablated rectangular hole. It impressively shows how the debris, which is caused by this *indirect* redeposition mechanism, renders the unwettable native PET (zone A) wettable (zone B). We see that zone B is covered by a thin film of water indicating a high-energy surface as for example fused silica. The form of the outer border of the wetted region in Fig. 3 corresponds very well to the form of the debris pattern, as also observed after excimer laser ablation of polyimide (PI) [13].

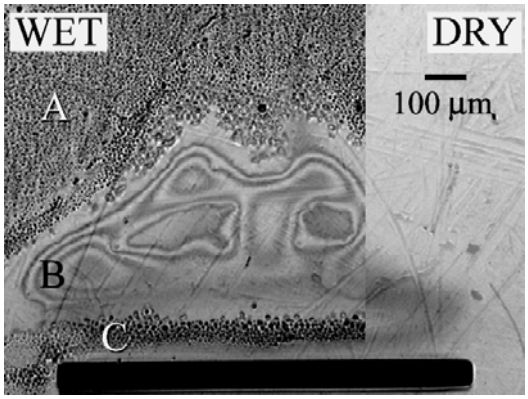

Fig. 3 Optical microscope image of water condensed by breathing out near a statically ablated surface in PET (200 pulses, 1000 mJ/cm^2, depth 38 µm). **Zone A:** non-wetting native PET. The dark dots are water droplets. **Zone B:** wetted surface because of redeposition by collision; we see a thin film of water. **Zone C:** non-wetting surface because of PLD-like direct redeposition. We see once more droplets of water. On the right side (dry image) we see only the main debris hill.

However, in scanning excimer laser ablation with high ramp angles we need to consider a second deposition pathway for the debris in the channels. This is a kind of "self-PLD" (PLD – pulsed laser deposition), where the substrate (channel floor) is approaching more and more the target (end ramp) for higher ramp angles [5]. Obviously, the angular density distribution in our case will not obey the simple $\cos^n(\theta)$-relation [14], as it does in PLD. The two main reasons for this are (i) the presence of the air and (ii) the irradiation of a relatively large rectangular surface, i.e. the inclined ramp. Nevertheless, it is reasonable to assume that inclining the irradiated surface with respect to the channel floor strongly enhances the direct deposition of ablation

products on the channel floor. This means that this kind of debris deposits on the channel floor without collisions with the oxygen-containing atmosphere. In consequence, this kind of debris will have a low ζ-potential.

For static ablation we can also observe in Fig. 3 (left part) a small region (zone C) directly at the border of the ablated surface where this kind of debris determines the surface properties, and the water cannot wet the surface. The comparison with the dry image shows that the borderline between zone B and C crosses the middle of the main debris hill, which has a homogenous surface topography as measured by AFM [15]. Thus, the wettability contrast between zones B and C, as described above, is due to a difference in chemical composition of the surfaces. In consequence, the non-wetting behavior of zone C cannot be attributed to a roughness effect [10].

Though, the maximum electroosmotic flow velocity appears at the ramp angle where we have the most redeposition by collision and still negligible PLD-like redeposition in the channel. The increase in electroosmotic flow velocity with increasing the ramp angle from $\alpha = 2.0°$ to $\alpha = 4.3°$, is caused by a change of the indirectly redeposited debris pattern. Miotello *et al.* have shown that the gas dynamic effects tend to result in a debris pattern, that is rotated with respect to the ablated shape [13]. Thus, little debris is deposited near to the short side of an ablated rectangular surface (Fig. 3). This effect will be more important for the spot of 40 μm × 1000 μm ($\alpha = 2.0°$) than for 40 μm × 500 μm ($\alpha = 4.3°$). Thus the usage of the 500 μm long spot enhances indirect redeposition at the short side of the rectangle, i.e. in the channel.

For $\alpha \geq 11°$, the PLD-like redeposition process becomes more and more important. The debris with low ζ-potential, deposited by this mechanism thus decreases the electroosmotic flow velocity.

5. Conclusions and Outlook

We showed that the electroosmotic flow in excimer laser ablated micro fluidic channels in PET varies with the ramp angle α. We obtained in stretched and unstretched PET-foils, i.e. with and without micrometric structures, a maximum flow velocity at a ramp angle of $\alpha = 4.3°$. The flow velocity, at this maximum, is comparable to the electroosmotic flow in fused silica.

The existence of the maximum flow velocity at $\alpha = 4.3°$ is attributed to the competition of two different debris redeposition mechanisms. The indirect redeposition occurs because of collisions of the ejected material with the surrounding gas molecules and deposits material with a high ζ-potential. The direct redeposition is a kind of PLD-mechanism. A part of the ablated material is directly ejected in the direction of the channel floor and forms material with a low ζ-potential on it. Direct redeposition becomes important at $\alpha = 11°$ and is dominant at $\alpha \geq 22°$. The existence of these two redeposition mechanisms was pinpointed by the water wetting experiment of the surroundings of a statically ablated rectangle in PET.

Finally, all electroosmotic flow velocities were measured in channels with a PE on PET lamination. This means that about a quarter of the channel walls is identical in all channels. Thus the variations in the ζ-potential of the ablated surfaces are higher than 25%. The ζ-potential values, of ablated surface and lamination, will be determined in the near future, by applying the formula of Andreev *et al.* [16].

6. Acknowledgements

This work was done in collaboration with the Laboratory of Electrochemistry of the Swiss Federal Institute of Technology Lausanne (EPFL). Especially we acknowledge François Bianchi for installing the electroosmosis setup and valuable discussions on the subject. Our thanks also go to the Swiss Federal Institute of Technology Lausanne (EPFL) for funding this work.

References

[1] J.S. Rossier, M.A. Roberts, R. Ferrigno and H.H. Girault: Anal. Chem., **71**, (1999), 4294-4299.
[2] Y. Kawamura, K. Toyoda and S. Namba: Appl. Phys. Lett., **40**, (1982), 374-375.
[3] J.S. Rossier, P. Bercier, A. Schwarz, S. Loridant and H.H. Girault: Langmuir, **15**, (1999), 5173 - 5178.
[4] F. Wagner and P. Hoffmann: Appl. Surf. Sci., **154-155**, (2000), 627-632.
[5] F. Wagner and P. Hoffmann: Appl. Phys. A, **69**, (1999), S841-S844.
[6] E. Arenholz, V. Svorcik, T. Kefer, J. Heitz and D. Bäuerle: Appl. Phys. A, **53**, (1991), 330.
[7] X. Huang, M.J. Gordon and R.N. Zare: Anal. Chem., **60**, (1988), 1837-1838.
[8] M.A. Roberts, J.S. Rossier, P. Bercier and H. Girault: Anal. Chem., **69**, (1997), 2035.
[9] S. Lazare and R. Srinivasan: J. Phys. Chem., **90**, (1986), 2124-2131.
[10] F.M. Fowkes: *"Contact Angle, Wettability, and Adhesion"* (American Chemical Society, Washington D.C., 1964).
[11] H. Niino and A. Yabe: Appl. Phys. Lett., **60**, (1992), 2697.
[12] S. Küper and J. Brannon: Appl. Phys. Lett., **60**, (1992), 1633.
[13] A. Miotello, R. Kelly, B. Braren and C.E. Otis: Appl. Phys. Lett., **61**, (1992), 2784.
[14] S. Lazare and V. Granier: Chem. Phys. Lett., **168**, (1990), 593.
[15] F. Wagner and P. Hoffmann: to be published, (2000).
[16] V.P. Andreev, S.G. Dubrovsky and Y.V. Stepanov: J. Micro. Sep., **9**, (1997), 443 - 450.